

DARK ENERGY AND DARK MATTER HALOS

Michael Kuhlen⁽¹⁾, Louis E. Strigari⁽²⁾, Andrew R. Zentner^(3,4), James S. Bullock^(5,7), and Joel R. Primack⁽⁶⁾

(1) Department of Astronomy and Astrophysics, University of California at Santa Cruz, 1156 High Street, Santa Cruz, CA 95064

(2) Department of Physics, The Ohio State University, 174 W. 18th Avenue, Columbus, OH 43210

(3) Center for Cosmological Physics, The University of Chicago, 5640 S. Ellis Avenue, Chicago, IL 60637

(4) Department of Astronomy and Astrophysics, The University of Chicago, 5640 S. Ellis Avenue, Chicago, IL 60637

(5) Harvard-Smithsonian Center for Astrophysics, 60 Garden Street, Cambridge, MA 02138

(6) Physics Department, University of California at Santa Cruz, 1156 High Street, CA 95064

(7) Hubble Fellow

Draft version December 21, 2018

ABSTRACT

We investigate the effect of dark energy on the density profiles of dark matter halos with a suite of cosmological N-body simulations and use our results to test analytic models. We consider only constant equation of state models of dark energy, and allow both $w = 1$ as well as models with $w < 1$. Using N simulations with w ranging from -1.5 to 0.5 and with more than 1600 well-resolved halos each, we show that the halo concentration model of Bullock et al. (2001) accurately predicts the median concentrations of halos over the range of w , halo masses, and redshifts that we are capable of probing. We find that the Bullock et al. (2001) model works best when halo masses and concentrations are defined relative to an outer radius set by a cosmology-dependent virial overdensity. For a fixed power spectrum normalization and fixed-mass halos, larger values of w lead to higher concentrations and higher halo central densities, both because collapse occurs earlier and because halos have higher virial densities. While precise predictions of halo densities are quite sensitive to various uncertainties, we make broad comparisons to galaxy rotation curve data. At fixed power spectrum normalization (fixed σ_8), $w > 1$ quintessence models seem to exacerbate the central density problem relative to the standard $w = 1$ and models with $w < 1$ help to reduce the apparent discrepancy. For example, models with $w = 0.5$ seem disfavored by the data, which can be matched only by allowing extremely low normalizations of $\sigma_8 < 0.6$ in this case, while models with $w = -1.5$ can more easily accommodate the observational data. We confirm that the Jenkins et al. (2001) halo mass function provides an excellent approximation to the abundance of halos in our simulations for $w = 1$. In our $w = -1.5$ simulation, we find that the Jenkins mass function underestimates the number of massive halos at high redshift, with the discrepancy exceeding 50% by $z = 1$ and growing larger with increasing redshift.

Subject headings: cosmology: theory { dark matter { large-scale structure of universe { methods: N-body simulations

1. INTRODUCTION

In the prevailing model of galaxy formation, galaxies assemble and evolve in the potential wells established by gravitationally bound halos of cold and collisionless dark matter (CDM). Except for some possible difficulties on small scales, the CDM model is remarkably successful in explaining a large number of observations. However, this success requires an additional "dark energy" component that drives an accelerated cosmic expansion to be added to the universal energy budget. While the presence of dark energy is firmly established observationally (see below), measuring its equation of state as well as developing a theoretical understanding of the nature of the dark energy are two of the biggest outstanding problems in cosmology today. Dark energy not only affects the large-scale evolution of the Universe, but also the collapse histories and density structures of dark matter halos. Understanding the precise nature of these effects is important for studies that aim to quantify the nature of dark energy using strong (e.g., Sarbu, Rusin, & Ma 2001; Huterer & Ma 2004; Kuhlen, Keeton, & Madau 2004) and weak (e.g. Hu & Jain 2003; Bartelmann et al. 2002) gravitational lensing. Changing the dark energy model should similarly change expectations for galaxy rotation

curves, and could either exacerbate or relieve one of the main small-scale problems facing CDM { the central-density problem (e.g., Zentner & Bullock 2002; McGaugh, Barker, & de Blok 2003, and references therein). In the present paper, we use a suite of N-body simulations to study how halo density profiles change as a function of dark energy equation of state, discuss our results in the context of analytic models, and extend our findings to discuss the observational implications of dark energy on galaxy scales.

The existence of some form of dark energy is supported by a preponderance of data. Taken together, observations of the magnitude-redshift relation of type Ia supernovae (SN Ia; Perlmutter et al. 1999; Riess et al. 2001; Knop et al. 2003; Barris et al. 2003), the power spectrum of cosmic microwave background (CMB) anisotropy (Spergel et al. 2003; Tegmark et al. 2003a), the power spectrum of galaxy clustering (Dodelson et al. 2003; Tegmark et al. 2003b), and the luminosity function and baryon fraction of clusters (Allen et al. 2003) provide nearly unimpeachable evidence for the existence of dark energy. The most common supposition is that the dark energy takes the form of a cosmological constant or vacuum energy. In this case, the energy den-

sity, and pressure p , are related through $p = -\rho$. An attractive alternative candidate for the dark energy is the potential energy of a slowly-varying scalar field, or "quintessence" (e.g., Ratra & Peebles 1988; Caldwell, Dave, & Steinhardt 1998).

A convenient parameterization of the dark energy is through an equation of state $w = p/\rho$ relating its energy density and pressure. In general, the equation of state parameter w is time-varying, but it is useful to model quintessence with a constant equation of state parameter because current observational data sets have limited power to distinguish between a time-varying and constant equation of state (e.g., Kujat et al. 2002). Useful limits on the equation of state for the dark energy, assuming that it remains constant in time, come from SN Ia studies, $1.67 < w < 0.62$ (Tegmark et al. 2003), and can be refined by combining SN Ia data with CMB anisotropy and galaxy clustering statistics yielding $1.33 < w < 0.79$ at $z = 2$ (Tegmark et al. 2003b). For our simulations, we adopt an empirical view and study five models that span a comparably large range of parameter space: $w = -1.5; -1.25; -1.0; -0.75; -0.5$.

Our theoretical understanding of halo profiles has improved recently largely through numerical simulations, performed in the context of CDM plus cosmological constant (CDM) or standard CDM (SCDM, i.e. $\Lambda = 0$, $\Omega = 0$) cosmologies (Navarro, Frenk, & White, 1995, 1996, 1997, hereafter NFW; Klypin, Klypin, & Klychkov 1997; Gigna et al. 1998; Jing 2000; Bullock et al. 2001; Eke, Navarro, & Steinmetz 2001; Wechsler et al. 2002, hereafter W02; Zhao et al. 2003; Hayashi et al. 2003; Navarro et al. 2003; for a review, see Primack 2003). It is generally understood that the final density profiles of halos are linked closely to their formation histories. Halo central densities are set during an early, rapid-accretion phase, and tend to be proportional to the density of halos in the Universe at the time of this rapid collapse (W02; Zhao et al. 2003; Tasitsiomi et al. 2003). Larger values of w lead to earlier collapse times and also to more rapid collapse of overdensities, thus we expect halos with higher relative central densities and higher virial densities (see our discussions in x2 and x3). In x4-6 we quantify these effects and test the expected scalings. We verify that the analytic technique of Bullock et al. (2001, B01) for predicting halo concentrations works well when applied straightforwardly to constant w cosmologies.

Testing this analytic model is important, because it allows us to extend our results to examine the effects of other model parameters. We remark that w correlates in a straightforward way with halo concentration only when the power spectrum normalization δ_8 is fixed. However, for a fixed value of w , higher or lower normalizations produce earlier and later collapse times respectively, and halo densities change correspondingly (x3.2). Unfortunately, the power spectrum normalization is the largest uncertainty in predicting concentrations and central densities and we discuss the impact of different normalizations in x5.2.

A related issue is the effect of dark energy on the halo mass function. Although it is not directly observable, theoretical insight into the expected halo mass function is attainable through current N-body simulations. The effects of dark energy on halo mass functions

have been investigated by Bartelmann, Perrotta, & Baccigalupi (2003), Linder & Jenkins (2003), Klypin et al. (2003), Maccio et al. (2003), and Lokas, Bode, & Homan (2003) and the accurate prediction of halo mass functions as well as accretion histories and density structures over a large range of redshifts is necessary in order to take full advantage of the ability of upcoming cluster surveys, such as the Sunyaev-Zeldovich Array (<http://astro.uchicago.edu/sza/>) to constrain the dark energy equation of state (see Carlstrom, Holder, & Reese 2001 for a review). There appears to be general agreement that halo mass functions can be approximated accurately by the "universal" mass function of Jenkins et al. (2001, hereafter J01) even in models with dark energy. In x5.1, we compare the results of previous studies of quintessence cosmologies with $w > -1$ and we report a potential discrepancy between the J01 mass function and simulation results for our model with the lowest $w = -1.5$ and at redshifts greater than $z = 1$.

Klypin et al. (2003) and Dolag et al. (2003) have performed previous numerical studies of CDM halos in quintessence cosmologies. Here our study overlaps with these, our results are in general qualitative agreement. This study extends, complements, and improves upon previous studies in several ways. We have assembled large catalogues of halos, with masses and concentrations for more than 1600 halos in each simulation. With this large number of halos we are able to measure halo distribution functions and quantitatively test the predictions of the B01 model for both the mean relation between concentration and mass and the halo-to-halo scatter. We also extend the mass range probed and extend the range of quintessence parameter space probed by simulations by exploring two models with $w < -1$.

The format of this paper is as follows. After a brief review of the basics of structure formation in models with dark energy in x2, we go on in x3 to describe the effects of constant w models on the analytic B01 model for halo concentrations. Then in x4 we describe the set of numerical simulations that we have performed. In x5, we present the mass functions and concentrations of CDM halos in these simulations. In x6, we briefly discuss the central density problem of CDM in light of our results. In x7, we present a summary of our findings, compare this work to previous studies, and discuss the implications of this work. Throughout this paper, we assume a flat universe with present matter density relative to critical of $\Omega_m = 0.3$, and Hubble parameter $h = 0.7$. The quintessence energy density is then $\rho_q = 1 - \Omega_m = 0.7$. We refer to a model with a cosmological constant ($w = -1$) as CDM. We use the terms "quintessence" and "QCDEM" to refer to all models which have $w \neq -1$.

2. STRUCTURE FORMATION IN QUINTESSENCE COSMOLOGIES

In this Section, we present a brief overview of the growth of structure in quintessence cosmologies. In x2.1, we introduce the basic results of cosmological perturbation theory with quintessence and discuss our computations of the matter power spectrum. We briefly discuss the normalization of the power spectrum in x2.2. A convenient way to define the mass and radius of a dark matter halo is through a mean overdensity δ_{vir} , relative to

the background density (see x3.1). The idea is to choose ν_{vir} so as to delineate the boundary between virialized and in-falling material. The equivalent linear overdensity at collapse δ_c is a quantity that is used to delineate the mass scale of objects that are forming at a particular redshift. Often, these overdensity criteria are chosen with reference to the evolution of a spherical tophat overdensity. In x2.3, we discuss the spherical tophat model in quintessence cosmologies.

We explore both conventional quintessence models with $w = 1$ and, adopting an empirical approach, we pursue models with $w < 1$. Requiring the kinetic energy of the quintessence to be positive imposes the condition $w > 1$ on the quintessence equation of state. When $w > 1$ and constant, all computations can be performed knowing only the value of w by assuming that the scalar field Lagrangian has a kinetic term of the canonical form. To explore the parameter space $w < 1$ consistently, we must choose a particular model for the scalar field dynamics and one simple possibility is a Lagrangian with a non-canonical kinetic term that differs from the canonical case by a negative sign. Explicitly, we adopt the "phantom energy" Lagrangian for the field, $\mathcal{L} = -\rho V$ (Caldwell 2002; Carroll, Hoyle, & Trodden 2003). Having made this choice, we can then express the derivatives of the potential completely in terms of w (Davé, Caldwell, & Steinhardt 2002).

2.1. Cosmological Perturbations

Here we consider linear perturbations to the CDM density field, $\delta(x) = \delta_b + \delta_m$, with δ_b the mean density of dark matter in the universe. Computing the linear evolution $\delta(x)$ requires solution of the linearized Einstein-Boltzmann equations (e.g., Ma & Bertschinger 1995). We perform our calculations in the synchronous gauge with a modified version of the publicly-available Einstein-Boltzmann code CMBfast by Seljak & Zaldarriaga (1996). We assume a scale-invariant spectrum of adiabatic primordial density fluctuations and a baryon density $\Omega_B h^2 = 0.02$.

The linear equation for fluctuations in the quintessence field in Fourier space is

$$+ 3H\dot{\delta} + (\dot{a}^2 - V; \dot{\delta}) = \pm [(1+w_Q)]^{1/2}; \quad (1)$$

where $V; \dot{a}^2 = \dot{a}^2$, $\dot{\delta}$ is the mean energy density in the quintessence field, and the plus (minus) signs correspond to fields with positive (negative) kinetic energy. Here the dots represent derivatives with respect to cosmological proper time t , and δ is the linear CDM fluctuation in Fourier space. From the evolution of the linear CDM fluctuation we can obtain the power spectrum, $P(k) = \delta(k)^2$. The CDM transfer functions for our scale-invariant primordial spectrum are defined from

$$P(k; z) = A_Q k T^2(k; z) \frac{D^2(z)}{D^2(0)}; \quad (2)$$

where A_Q is the normalization and $D(z) = (z)/(z=0)$ is the linear growth factor. On scales larger than the Compton wavenumber, $k_Q = \sqrt{V}$, δ can grow and, in turn, act as a source for the evolution of δ . On small

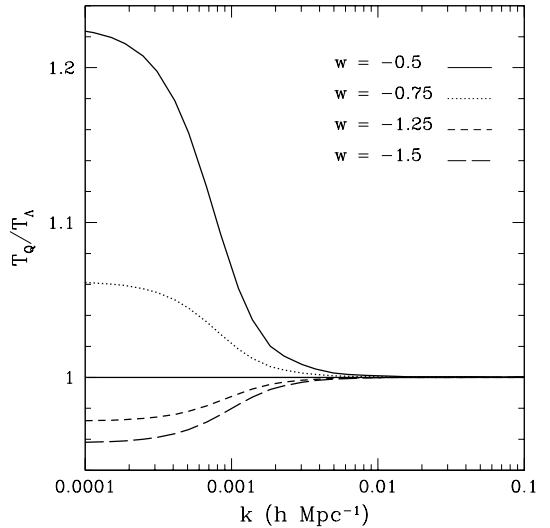


Fig. 1. The ratio of $z = 0$ quintessence transfer functions to CDM for different models. The transfer functions are similar for wavenumbers $k < 0.01 h \text{ Mpc}^{-1}$. The different equation of state parameters are shown in the legend.

scales $k > k_Q$, perturbations in the quintessence field decay, so the CDM transfer functions retain the form from CDM, while on scales $k < k_Q$, the form of the transfer functions reflect the clustering of matter (Ma, Caldwell, Bode, & Wang). Figure 1 shows the ratio of the CDM transfer functions with quintessence, T_Q , to the transfer function in the corresponding CDM model ($w = 1$), T , at $z = 0$. For $k < k_Q$ and $w < 1$, the gravitational source from the quintessence field, $\delta \propto k^3$, sources the growth of δ . For $w > 1$, the source from the quintessence field changes sign, resulting in a decrease in the gravitational potential and in δ .

2.2. Power Spectrum Normalization

For a fixed cosmology and w , the most important parameter in setting the scale radii of halo density profiles is the normalization of the matter power spectrum on small scales. In our N-body experiments, we have chosen to normalize each model with a similar value of σ_8 , set by cluster abundance estimates. We do so because the abundance of clusters is a more direct probe of the amount of power on the scales that are relevant to galaxy formation than the CMB anisotropy measurement and in order to isolate the differences that arise because of variations in the expansion rate in models with different values of w .

We normalize the power spectrum to the abundance of massive clusters using x-ray flux and temperature measurements from the cores of clusters of galaxies and the corresponding conversion to cluster mass from the mass-temperature (M-T) relation. With all other cosmological parameters fixed, comparison of the observed mass function to the predicted mass functions from N-body simulations (J01) determine the normalization parameter σ_8 , which is the rms overdensity in spheres of radius $R = 8 h^{-1} \text{ Mpc}$. The quintessence field is smooth on scales much smaller than the horizon size, thus the values of σ_8 derived from $z = 0$ cluster scale measurements

have very small w dependence.

Currently, the largest source of error in the determination of σ_8 from clusters is the uncertainty in the normalization of the $M-T$ relation. Numerical simulations consistently measure the normalization a factor of 2 greater than that observed from x-ray temperature data (e.g., Seljak 2002 and references therein). For CDM and $M = 0.3$, our current understanding of the $M-T$ relation places σ_8 very broadly in the range $0.65 < \sigma_8 < 1.1$ (Pierpaoli, Scott, & White 2001; Reiprich & Böhringer 2002; Pierpaoli et al. 2003). Using the HIFLUGCS cluster mass function (Reiprich & Böhringer 2002) we find for $M = 0.3$, $\sigma_8 \approx 0.74$, very nearly independent of w (Kuhlen, Keeton, & Madau 2004). We normalize the power spectra to $\sigma_8 = 0.742; 0.740; 0.738; 0.736; 0.734$ for $w = 1.5; 1.25; 1.0; 0.75; 0.50$. In principle the value of σ_8 as determined from clusters is degenerate with M (e.g. Schuecker et al. 2003), indeed for analysis of the HIFLUGCS sample the global best fit is $M \approx 0.12$, $\sigma_8 \approx 0.96$ in a CDM cosmology; however, we adopt values of σ_8 that best fit the data given our choice of $M = 0.3$.

While we have chosen to normalize our numerical simulations using the cluster abundance, this normalization is fairly uncertain and in the interest of completeness we remark that not all of these model normalizations are consistent with $n = 1$ normalization to CMB anisotropy (even modulo uncertainties in the reionization epoch). In the simplest case, with all other cosmological parameters held fixed, the value of w affects the CMB-derived σ_8 normalization primarily through the late-time integrated Sachs-Wolfe (ISW) effect (see Hu & Sugiyama 1995). For universes with $w < 1$, the quintessence energy density becomes comparable to that of CDM at earlier epochs relative to CDM, resulting in greater variation in the gravitational potentials along lines of sight to the surface of last scattering. For lower values of w , the ISW effect is not as prominent because quintessence becomes dynamically important only at more and more recent epochs. In Figure 2, we show the value of σ_8 implied by the CMB normalization as a function of the equation of state parameter w . As we stated above, the decrease in σ_8 is due to the increased importance of the ISW effect as w increases.

Care must be taken when setting the CMB normalization. First, we note that when we performed our N-body experiments we fixed the parameter $M = 0.3$ for all models rather than allowing M to vary along the $M-w$ degeneracy in the angular diameter distance or the luminosity distance. Our most extreme models are currently disfavored by the present observational data (e.g., Tegmark et al. 2003; Knap et al. 2003), but as our intent is to address the effect of quintessence on structure and halo formation, we do not consider this to be a serious deficiency. Also, in principle the WMAP (Spergel et al. 2003) result of high optical depth to the last scattering surface τ , has made the determination of σ_8 from the CMB less robust, as the scattering of free electrons dampens isotropies on scales that are sub-horizon at the epoch of reionization, thereby introducing a degeneracy between τ and σ_8 . The dashed line in Figure 2 shows the CMB-normalized σ_8 as a function of w implied by

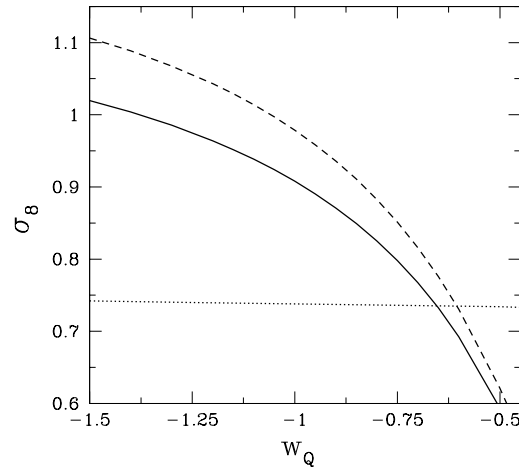


Fig. 2. The power spectrum normalization σ_8 , implied by CMB anisotropy as a function of w . The solid line shows the values of σ_8 that we obtain by assuming the optical depth to the last scattering surface $\tau = 0$. The dashed line shows the values of σ_8 implied by adopting $\tau = 0.17$. The dotted line shows the values of σ_8 that we infer from the abundance of massive x-ray clusters.

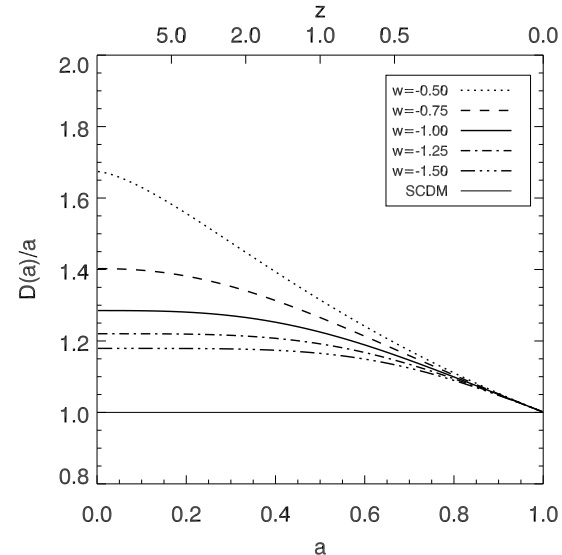


Fig. 3. Ratio of the growth factor to the SCDM growth factor $D_{SCDM}(a) = a$ as a function of scalefactor for different values of w . The growth factor is normalized to unity today ($D(a = 1) = 1$). Linetypes are shown in the legend.

adopting an optical depth to the last scattering surface of $\tau = 0.17$, in line with the WMAP expectations.¹

We return to a discussion of the relative importance of σ_8 and w in x6-8.

¹ Note that a high optical depth to reionization appears to be difficult to reconcile with low values of σ_8 . $\sigma_8 \approx 0.75$ (e.g., Somerville, Bullock, & Livio 2003), though the CMB-derived σ_8 is very uncertain and is somewhat degenerate with the tilt of the power spectrum, so tilted models with low σ_8 may still be viable. This issue will likely be settled with future CMB data and analysis.

2.3. The Spherical Collapse Approximation

A common convention is to define the virial mass and radius of a dark matter halo by demanding that the mean density within the virial radius of the halo be a factor Δ_{vir} times larger than the background density, ρ_b . Thus the virial mass and radius of a halo are related by

$$M_{\text{vir}} = \frac{4}{3} \Delta_{\text{vir}} \rho_b R_{\text{vir}}^3 : \quad (3)$$

In addition, the equivalent linear overdensity at collapse $\delta_c(z)$ is often used to determine the mass scale that is typically collapsing at a given epoch. Both of these overdensities can be estimated using the approximation of spherical top-hat collapse (e.g., Lacey & Cole 1993). We extend these results to quintessence cosmologies in this section.

The evolution of linear overdensities on scales much smaller than those on which the quintessence field spatially clusters is

$$+ 2H(a) - \frac{3}{2} H_0 M a^3 : \quad (4)$$

Solving this equation gives the growth factor for linear perturbations. Figure 3 shows the linear growth factor in five different quintessence models, normalized to the growth factor in an $M = 1$ SCDM cosmology in which $D(a)/a$. As w increases in the quintessence models, the growth of structure occurs relatively earlier.

Initially an overdensity is linear and expands with the background. Eventually the growing overdensity becomes non-linear ($\delta > 1$), breaks away from the cosmological expansion, and "turns around" to collapse. The object subsequently virializes at a virial overdensity Δ_{vir} , which can be determined using the virial theorem along with an estimate of the potential energy density of the matter and the quintessence field associated with the overdensity at the time of turnaround. We follow Wang & Steinhardt (1998) and Weinberg & Kamionkowski (2003) and use the spherical collapse approximation in order to estimate these quantities and to determine how $\Delta_{\text{vir}}(z)$ varies with w .

Consider an initial overdensity patch δ_{ta} at the time of turnaround ($R = 0$) with radius R_{ta} . If we define $y = R/R_{\text{ta}}$ as the ratio of the radius of the overdense region to its initial radius, the momentum component of the Einstein equations give:

$$y = \frac{1}{2} \frac{(1 + \delta_{\text{ta}}) H_{\text{ta}}^2 M_{\text{ta}}}{y^2} \frac{3}{2} \left(\frac{1}{3} + w \right) \rho_0 H_0^2 Y (1 + z)^{3(1+w)} : \quad (5)$$

The subscript "0" specifies quantities evaluated at the present epoch. The overdensity is said to collapse as $y \rightarrow 0$. The non-linear overdensity at collapse is determined by assuming the overdense region collapses at the time t_{coll} when $y \rightarrow 0$ in equation (5), but that the final radius of the collapsed object is finite and can be computed using the virial theorem. We compute the equivalent linear overdensity at collapse by evolving the linearized equation of motion of the overdensity [Eq. (4)] until the time t_{coll} given by the non-linear evolution of the overdensity. In the CDM cosmology, the linear and

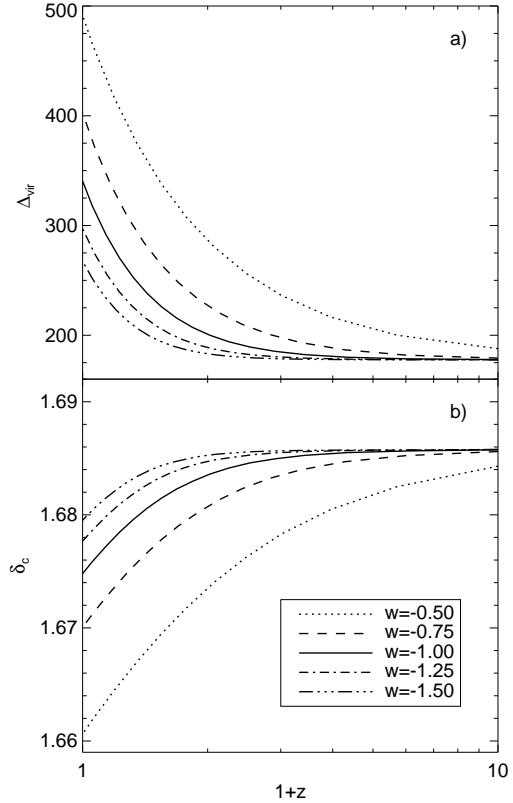


Fig. 4. | The non-linear and linear overdensities at collapse in quintessence cosmologies. In panel (a), we exhibit the non-linear overdensity at collapse $\Delta_{\text{vir}}(z)$ for 5 different quintessence models that we explore in this paper ($M = 0.3$). The different values of the quintessence equation of state parameter w , are shown in the legend. The increase in $\Delta_{\text{vir}}(z)$ for larger w results primarily from later collapse redshifts. In panel (b), we show the equivalent linear overdensity at collapse $\delta_c(z)$, as a function of redshift for the same quintessence models.

non-linear overdensities at collapse are $\delta_c(z = 0) \approx 1.67$ and $\Delta_{\text{vir}} \approx 337$ and vary with redshift. In SCDM, these quantities are $\delta_c \approx 1.686$ and $\Delta_{\text{vir}} \approx 178$ and are not functions of redshift.

We present our results for the equivalent linear overdensity at collapse $\delta_c(z)$, and the non-linear overdensity at collapse $\Delta_{\text{vir}}(z)$ as a function of redshift in quintessence cosmologies in Figure 4. The trend in $\delta_c(z)$ reflects the fact that overdensities grow more slowly in higher- w models. We can understand the behavior of $\Delta_{\text{vir}}(w; z)$ by noting that overdensities in models with larger w will take longer to collapse, especially at late times. Consider, for example, two halos, one in a $w = -1$ cosmology, and another in a $w > -1$ cosmology, both of which are just virializing at some redshift z . Very roughly speaking, the $w > -1$ halo will have had a turn-around time at a higher redshift than the $w = -1$ halo, and its virial density will be higher to reflect this. Conversely $w < -1$ models will have more recent turn-around times and smaller virial overdensities. We find that an accurate fitting function including the regime $w < -1$ is

given by a slight modification to the formula already provided by Weinberg & Kamionkowski (2003) for $w > 1$ quintessence,

$$v_{\text{vir}}(z) = 18^2 \frac{1}{1+a} \frac{1}{1+b(z)}; \quad (6)$$

where $(z) = 1$, and with $a = 0.4316 \frac{1}{2} (z) \frac{0.2342}{1}$ and $b = 0.9287 \frac{1}{0.2215} (z) \frac{0.7274}{1}$. We find this fitting function accurate to better than 2% for $0.1 \leq z \leq 1$ and $0.5 \leq w \leq 1.5$.

It is important to stress that by adopting Eq. (3) as our definition of halo mass, we implicitly assume that all halos are just collapsing and virializing at the time of observation, z . In the next section we discuss a different type of collapse time, the "rapid-collapse epoch", which, in principle, is distinctly different from the halo turnaround time. The turnaround time refers to the halo as a whole. On the other hand, the rapid collapse epoch is associated with an earlier period when the central regions of the halo were being built up. As explained below, these two epochs are related to physically distinct phenomena, and both seem to play a role in setting halo densities: the first controls the average density within the halo virial radius, and the second controls the relative difference between the halo central density and its virial density.

3. ANALYTIC MODEL FOR HALO CONCENTRATIONS

3.1. Main Ingredients

Although numerical studies have revealed that dark matter halos in general are not spherical (Monaco 1995; Lee & Shandarin 1999; Sheth & Tormen 1999; J01; Bullock 2002; Jing & Suto 2002; Flores, Bullock, Klypin, & Primack 2004) and weak gravitational lensing seems to confirm this prediction (Hoekstra, Yee, & Gladders 2003), it is nonetheless useful to describe their density profiles with a simple, spherically-averaged two parameter model. It is now commonly agreed that in the absence of baryons, the density profiles of dark matter halos can be described fairly well by a generalized NFW profile on scales that are resolved in state-of-the-art N-body simulations:

$$\rho_{\text{halo}}(r) = \frac{s}{(r=r_s) (1 - r=r_s)^3}; \quad (7)$$

where s describes the slope of the inner density profile at $r < r_s$. The value of s that most closely represents the results of N-body simulations is still somewhat uncertain, with acceptable values lying somewhere between 0.7 and 1.5. An additional complexity is that recent studies indicate that halos of a given mass exhibit a range of inner slopes (Klypin et al. 2001; Tasitsis et al. 2003; Navarro et al. 2003). In the following, we have adopted a value of $s = 1$, corresponding to the original NFW proposal. In this paper we are concerned with the concentration parameter c_{vir} (see below), which is quite insensitive to the exact value of s .

The two parameters of the NFW profile are r_s and s , with r_s the radius at which the logarithmic density slope becomes equal to -2 . The concentration of the halo is defined as the ratio of its virial radius to the scale radius of the NFW profile,

$$c_{\text{vir}} = \frac{R_{\text{vir}}}{r_s}; \quad (8)$$

With these definitions the halo virial mass is related to the density parameters via

$$M_{\text{vir}} = 4 \pi r_s^3 \ln(1 + c_{\text{vir}}) \frac{c_{\text{vir}}}{1 + c_{\text{vir}}}; \quad (9)$$

Thus the halo density profile is also completely determined by specifying M_{vir} and c_{vir} .

Numerical simulations have revealed a strong correlation between M_{vir} and c_{vir} , with halo concentrations log-normally distributed around the median relation. Several simple models have been developed to explain this correlation (NFW; B01; Eke, Navarro, & Steinmetz 2001). Here we focus on the B01 model and test the accuracy with which it reproduces the observed relation between halo mass and concentration, not only in CDM simulations, but also in simulations with $w \neq -1$.

The B01 model assumes that a halo's central density and concentration are set by the density of the universe at a characteristic formation epoch. This formation epoch qualitatively tracks the characteristic collapse time for the halo subunits. It is defined as the time when the linear mass density fluctuations at a scale corresponding to a fraction F of M_{vir} is equal to c , the linearly extrapolated overdensity at collapse in the spherical top-hat model:

$$(F M_{\text{vir}}; c) = c(c); \quad (10)$$

Given the halo formation epoch the halo concentration is set via

$$c_{\text{vir}}(M_{\text{vir}}; a) = K_{\text{vir}} \frac{a}{a_c(M_{\text{vir}})}; \quad (11)$$

While this model is quite simple, it provides a qualitative argument for why halo concentrations seen in N-body simulations scale as they do as a function of mass and redshift. For example, when rare, massive halos collapse, they typically are assembled from subunits that have themselves collapsed only recently, and cannot sink deeply within their host system in order to create a highly-concentrated core. This would suggest that massive halos will be much less concentrated than their lower-mass counterparts, which form out of dense subunits.

Interestingly, a more detailed investigation by Wechsler et al. (2002, W02) showed that the B01 "collapse epoch" seems to correspond closely to the epoch when the mass accretion rate of the halo $d \ln(M_{\text{vir}})/dt$, is large compared to the rate of cosmic expansion. Wechsler et al. (2002, W02) found that if one defines the end of this rapid collapse phase to be when $d \ln(M_{\text{vir}})/dt = \ln(a)/2$, then this corresponds closely to the "formation epoch" defined above. After this epoch of rapid mass accretion ends, the halo mass and virial radius continue to grow via primarily minor mergers and diffuse mass accretion. These relatively minor mergers do not affect the inner regions of the halo ($r < r_s$) significantly and so R_{vir} grows, but r_s remains approximately constant, leading to an increase in concentration as the halo evolves (W02).

The B01 model thus has two parameters, F and K , that have to be determined by calibrating them to numerical simulations. B01 analyzed two CDM N-body

simulations with different resolutions and box sizes. Using a halo finder based on the Bound Density Maxima (BDM) algorithm (Klypin & Holtzman 1997), they assembled a catalog of several thousand halos for each simulation, and the NFW profiles to each of them. The B01 model was able to satisfactorily reproduce the mean relation between halo mass and concentration and its redshift dependence with $F = 0.01$ and $K = 4.0$.

The most thoroughly studied simulation in B01 was a CDM, $\sigma_8 = 1.0$, $60h^{-1}\text{Mpc}$ box, with a 512^3 grid and 256^3 particles, run with the Adaptive Refinement Tree (ART) code (Klypton, Klypin, & Khokhlov 1997). The mass per particle in this simulation was $1.1 \cdot 10^9 h^{-1}\text{M}_\odot$, and the force resolution at maximum refinement was equal to about $1.8 h^{-1}\text{kpc}$. In this simulation, B01 found that $K = 4.0$ and $F = 0.01$ reproduced the median $c_{\text{vir}}\text{-}M_{\text{vir}}$ relation very well over a range in halo masses from $M_{\text{vir}} \sim 2 \cdot 10^{11} h^{-1}\text{M}_\odot$ to $M_{\text{vir}} \sim 6 \cdot 10^{13} h^{-1}\text{M}_\odot$. B01 also quantified the scatter around this relation and determined that $\log c = 0.14 \text{ dex}$ (W02). Other numerical studies have found a somewhat smaller scatter, with Jing (2000) reporting $\log c = 0.09 \pm 0.11 \text{ dex}$, and Jing & Suto (2002) finding $\log c = 0.13 \text{ dex}$.

Note that the B01 model with $F = 0.01$ and $K = 4.0$ has proven successful in reproducing concentrations of CDM halos over more than six orders of magnitude in halo mass from $M_{\text{vir}} \sim 10^7 \text{ M}_\odot$ to $M_{\text{vir}} \sim 10^{13} \text{ M}_\odot$ (e.g., Colín et al. 2003, Hayashi et al. 2003). However, as discussed in B01, the model ceases to make physical sense for halo masses large enough that $F M_{\text{vir}}$ begins to approach the non-linear mass at $z = 0$. This is because linear fluctuations stop growing at late times in CDM, and with the simplified definition of collapse time discussed above, very large halos will never collapse. Consequently, the B01 model with $F = 0.01$ under-predicts halo concentrations for systems more massive than a few 10^{14} M_\odot (e.g. Hayashi et al. 2003, Dolag et al. 2003). As a matter of pragmatism, this result can be remedied with a simple change of parameters. With $F = 0.001$ and $K = 3.0$ the model works adequately for all masses of interest, although it becomes somewhat less attractive aesthetically because of the small value of F . For very massive halos that typically form recently, it may be more appropriate to set concentrations using the mass accretion history method of W02. With this method, the formation epoch can be determined directly from a mass-accretion history generated by the Extended-Press-Schechter formalism.

3.2. The Analytic Model in Quintessence Cosmologies

As shown in x2, linear overdensities have greater relative growth at higher redshift as w increases. We then expect, given an overdensity on a mass scale M_{vir} , that this mass scale will collapse at higher redshift as we increase w . As the halo concentration reflects the density of the universe at the time of rapid collapse, we expect this change in average formation time to translate directly into a change in average concentration. The differences in $w \neq -1$ models should be connected to changes in the rapid-collapse epoch a_c for halos of a given mass.

From Equation (10), a_c for a halo of mass M_{vir} is determined by c , $D(a)$, and σ_8 . The changes in c with w (Figure 4) have a very small effect on a_c . More relevant are the changes in $D(a)$ and the linear growth rate

(Figure 3). For a fixed value of σ_8 all the w -dependence of $a_c(M_{\text{vir}})$ will be captured by $D(a)$, with $M_{\text{vir}};a$ reaching the collapse threshold at earlier time for models with increasing w . More relative growth occurs during earlier epochs for models with higher w , causing mass scales to collapse when the universe is more dense. We therefore expect concentrations to increase as w increases.

Finally, note that a definition of concentration in terms of R_{200} , the radius at which the mean halo density is equal to 200 cm^{-3} (rather than r_{vir} for R_{vir}) has frequently been used in the past: $c_{200} = R_{200}/r_s$ (e.g., NFW 96). Of course, given a set of cosmological parameters, the model described above (as well as other analytic models like that of Eke et al. 2001) can be used to predict equivalent relations between c_{200} and M_{200} . For a fixed cosmology, the predicted relation between c_{200} and M_{200} will look quite similar to the c_{vir} vs. M_{vir} relation, with an offset that varies slowly as a function of concentration and accounts for the differences in values of the outer halo radius. The same holds true for fixed cosmologies of varying power spectrum normalization.

Because the simulations of B01 focused only on one cosmology, it was impossible to tell whether agreement with the simulations and the proposed B01 model was sensitive to the choice of defining halo concentration relative to R_{vir} instead of R_{200} . That is, one could have equally well proposed a different model based on c_{200} :

$$c_{200}(M_{200};a) = K_{200} \frac{a}{a_c(M_{200})}; \quad (12)$$

The simulation results of B01 could have been reproduced using this model, simply by setting K_{200} equal to a slightly smaller value than the original $K = 4.0$.

Consider now the current case, where we compare simulation results based on cosmologies with different w 's and hence different vir values. In these simulations, the ratios of R_{vir}/R_{200} (and c_{vir}/c_{200}) for fixed-mass halos will depend on the value $\text{vir}(w)$. Therefore, it is impossible for a model based on c_{200} with fixed K_{200} to do equally well as the original B01 model based on c_{vir} with fixed K for all values of w . More physically, the original B01 model described above implicitly assumes that the halos have virialized at the appropriate virial density and predicts that, in addition, the halo collapse redshift acts to set the ratio of the virial density ($/R_{\text{vir}}^3$) to the central density ($/r_s^3$). A model based on c_{200} with fixed K_{200} would instead assume that all of the changes in halo density arise solely because of changes in a_c . As demonstrated below, the virial assumption seems to capture better what happens in our N-body results. It seems therefore, that there are indeed two physical processes that set halo densities: one process is related to the global process of halo virialization and the other is related to an earlier, rapid-collapse epoch.

4. SIMULATIONS

In this section we describe the numerical simulations we have performed in order to investigate halo formation and structure in universes with quintessence. In x4.1 we explain the modifications to the publicly available N-body code GADGET (Springel, Yoshida, & White 2001). x4.2 details the numerical and cosmological parameters that were used in the simulations, and x4.4 describes the

process by which we locate halos and the NFW profiles to their density structures.

4.1. GADGET with Dark Energy

We use GADGET version 1.1, a publicly available and well-tested N-body code (Springel et al. 2001). Although it is possible to include hydrodynamics in the SPH formulation with this code, we have simulated only dissipationless dark matter particles. Gravity between particles is solved using a hierarchical tree algorithm in comoving coordinates, and both the force calculations and the time-stepping are performed in a fully adaptive way. Using the parallel version, we have run the code on either 96 375M Hz IBM Power3 processors of NERSC's Seaborg or on 64 1.4G Hz Athlon processors of Upstate, a 264-processor Beowulf cluster at The University of California at Santa Cruz.

Here we make the necessary alterations to the expansion rate of the universe for GADGET to account for quintessence cosmologies with $w \neq -1$. When normalizing δ on the scale of galaxy clusters, the initial power spectra are nearly unaffected by the inclusion of quintessence. However, when normalizing to the scales probed by the CMB, the initial power spectra are altered by the inclusion of quintessence (section 2.2). As discussed below, we normalize our simulations such that $\delta \approx 0.74$, thus the effect of $w \neq -1$ is due almost exclusively to the expansion rate.

4.2. Numerical and Cosmological Parameters

Power et al. (2003) have performed a detailed convergence study of a high resolution cluster simulation using GADGET, and although we simulate a much larger cosmological volume we have followed their recommendations for a number of GADGET's parameters. In particular we have chosen an adaptive timestep equal to $t_i = a_i - a_{i-1}$, where a_i and a_{i-1} are the gravitational softening and acceleration experienced by the i^{th} particle in the simulation, and a is a dimensionless constant. Power et al. (2003) recommend setting $a = 0.2$; this choice of adaptive timestep minimizes undesirable effects due to particle discreteness and hard scatterings, while at the same time allowing for convergence at minimal computational expense.

In order to prevent unphysical two-body relaxation effects from occurring, it becomes necessary to soften the gravitational potential at small scales. In GADGET this softening is performed using a cubic spline (Springel et al. 2001), for which the potential becomes exactly Newtonian at $r = 2.8$, where ϵ is the softening length. Generally our simulations were run with a comoving softening length of $\epsilon = 2.5h^{-1}$ kpc, although we have run a few cases with ϵ as low as $1h^{-1}$ kpc. Our cosmological background model is fixed by $M_m = 0.3$, $\Omega_0 = 0.7$, $h = 0.7$, and $n = 1.0$ for all values of w .

All of our simulations were run with 256^3 particles in boxes with sides of length $60h^{-1}$ Mpc. $M_m = 0.3$ implies a mass per particle of $M_p = 1.1 \times 10^9 h^{-1}$ M $_{\odot}$. For the analysis of halo concentrations we used only halos with more than 100 particles (see x5.2). This corresponds to a minimum halo mass of $M_{\text{vir}}^{\text{min}} = 1.1 \times 10^{11} h^{-1}$ M $_{\odot}$, for which the B01 model predicts a median concentration of 13.5 (for $\delta = 0.74$). This translates into an NFW

Table 1. Simulation Parameters and Power Spectrum Normalizations

Model w	$=h^{-1}$ kpc	$\delta_{\text{nom}}^{\text{a}}$	δ_{re} ^a
0.50	2.5	0.742	0.799
0.75	2.5	0.740	0.775
1.00	2.5	0.738	0.716
1.00	1.0	1.000	0.972
1.25	2.5	0.736	0.716
1.50	2.5	0.734	0.714

Note. | All other parameters are fixed at the same value for all simulations. The number of particles is $N_p = 256^3$, the box size is $L_{\text{box}} = 60h^{-1}$ Mpc, and the initial redshift is $z_i = 50$. For all simulations, the remaining cosmological parameters are $M_m = 0.3$, $\Omega_0 = 0.7$, $h = 0.7$, and $n = 1.0$.

^a the difference between δ_{nom} and δ_{re} is explained in x4.3.

scale radius of $r_s^{\text{min}} = 10h^{-1}$ kpc. More massive halos will have larger scale radii, and since even this minimum scale radius is almost three times larger than our softening length, we should be able to determine accurate concentrations from the halos in our simulations.

Table 1 summarizes the parameters used in our simulations.

4.3. Initial Conditions

Setting initial conditions for our simulations requires fixing the $z = 0$ normalization parameter, δ . From the linear growth function we can then determine the normalization of the spectrum at $z = 50$, the initial redshift of the simulations. As discussed above (x2.2), our current understanding of present day clusters of galaxies makes δ still uncertain by 20–30% ($\delta = 0.70$ –1.10 for $M_m = 0.3$). Halo concentrations in cosmological N-body simulations depend quite sensitively on δ , because it directly affects the halo formation time, especially for high mass halos. For example, at $M_{\text{vir}} = 10^{14} h^{-1}$ M $_{\odot}$ the B01 model predicts median concentrations of $c_{\text{vir}} = 6.8$ and $c_{\text{vir}} = 5.3$ for $\delta = 0.90$ and $\delta = 0.74$, respectively. For the simulations used in this paper, we initialize the simulations with the values of δ determined by Kuhlen et al. (2004) from the abundance of clusters in the HIFLUGCS sample of local clusters (Reiprich & Böhringer 2002): $\delta = 0.742; 0.740; 0.738; 0.736; 0.734$ for $w = 1.50; 1.25; 1.00; 0.75; 0.50$. We construct initial conditions for each w with the routines of the publicly available PM code (Klypin & Holtzman 1997). Figure 5 shows the resulting power spectra, determined from the initial condition data.

The process of converting a theoretical linear power spectrum into a set of particle positions and velocities is subject to statistical fluctuations. The largest modes of the system ($\sim L_{\text{box}}$) are only sampled once per dimension and are thus sensitive to deviations caused by small number statistics. Since $8h^{-1}$ Mpc is close to L_{box} , this can lead to noticeable differences between the nominal (δ_{nom}) input to construct the initial conditions and effective value (δ_{re}) determined from the actual particle positions of the initial conditions. Here we determine δ_{re} by direct numerical integration of the initial N-body power spectrum :

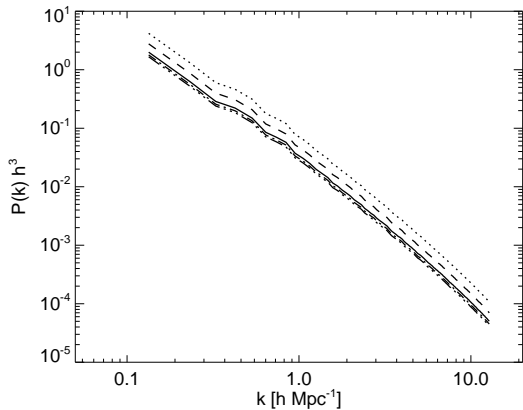


Fig. 5. The initial power spectra of the five simulations discussed in x5. From top to bottom w decreases from $w = 0.50$ to $w = 1.50$ in increments of $w = 0.25$. The spectra have been truncated just below the Nyquist wavenumber of the simulations, $k_{Ny} = 9.4 \text{ Mpc}^{-1}$.

$$\frac{2}{8_{\text{re}}} = \frac{1}{2} \frac{D^2(z=0)}{D^2(z=50)} \int_0^{z=1} k^2 P_{\text{num}}(k) W(kR_8)^2 dk; \quad (13)$$

where $P_{\text{num}}(k)$ is the power spectrum derived from the N-body initial conditions and $W(x)$ the spherical top-hat window function given by $W(x) = 3x^2(\sin x - x \cos x)$, evaluated at kR_8 , with $R_8 = 8h^{-1} \text{ Mpc}$.

$P_{\text{num}}(k)$ (Fig. 5) only extends down to k_{m} in $0.1h^{-1} \text{ Mpc}^{-1}$, which is not low enough to allow the integral in Equation 13 to converge. We estimated the portion of the integral below k_{m} by integrating the smooth universal power spectrum, and applied this correction to get 8_{re} . We found that for $w = 1.00$, $8_{\text{re}} = 0.715$, which is about 3% lower than 8_{nom} . However, the variation of 8 in a box of this size due to cosmological variance, should be roughly 6% so this difference is not surprising. We have constructed 1000 realizations of the initial conditions and explicitly verified that the values of 8 that we infer from these realizations are distributed with a standard deviation of approximately 6%. Therefore, the difference between 8_{re} and 8_{nom} for the three $w = 1$ cases is not surprising as it is well within the variation due to the finite volume of the simulation box. Similarly, we find $8_{\text{re}} = 0.775; 0.799$ for $w = 0.75; 0.50$, respectively, corresponding to 5% and 8% deviations. We used the same random number seed in the construction of all five initial conditions, therefore it is not possible to explain both the decrease in 8_{re} for $w = 1$ and the increase for $w > 1$ by statistical fluctuations in the largest modes. We have not been able to find the cause of this anomaly, and have concluded that it must be due to an error during the generation of the initial conditions. Our numerical simulations are quite computationally expensive, therefore we have decided not to re-simulate the two $w > 1$ cases. Instead, we used 8_{re} for the purpose of comparing our results to the analytic model of the previous section.

4.4. Halo Finders

We have used several different halo finding algorithms to locate the halos in our simulations depending upon the way in which we apply our simulation data. In x5.1, we compare the mass functions of our simulated halos with the J01 "universal" mass function. J01 used the Friends-of-Friends (FoF) algorithm (Davis et al. 1985) in order to find halos in simulations. In order to make a direct comparison to the J01 mass functions we have employed a University of Washington FoF halo finder (<http://www-hpcc.astro.washington.edu/tools/fof.html>). As in J01 we set the linking length to 0.2 times the mean particle separation, regardless of cosmology.

For a direct comparison in x5.2 of our N-body halo concentrations to the B01 model, we have employed an updated version of the halo finder that B01 and W02 used. This halo finder is based on the BDM algorithm (Klypin & Holtzman 1997), but extends it to remove particles that are not bound to the halo in question. Additionally, the code also fits NFW profiles to each of the halos and determines c_{vir} . For more detail we refer the reader to Appendix B of B01 and Appendix A of W02. We have included into our catalogs only halos with more than 100 particles, the same cut-off used by W02.

We have checked to see whether both halo finding algorithms agree with each other within our expectations by comparing mass functions. The systematic differences in total mass between halos defined in terms of the cosmology-dependent virial overdensity $\delta_{\text{vir}}(w)$ (as in the BDM-like finder) and those based on a fixed value of FoF linking length of 0.2 times the mean interparticle separation translate into only minor differences in mass functions. At high redshift the two mass functions actually converge because $\delta_{\text{vir}}(z)$ approaches 178 and a linking length of 0.2 times the mean interparticle separation corresponds, roughly speaking, to a mean halo density of 180–200 times the background density. Below $z = 2.25$, the FoF and BDM mass functions agree very well, but at higher redshifts the BDM-based finder becomes increasingly incomplete. A consequence of the low value of δ in our simulations is that halo formation occurs more recently. Frequent merger events during the rapid mass growth phase of halo formation will disrupt any spherical symmetry in the halo density profile. These halos will not be well described by the NFW formula. In our BDM halo finder, halos with very bad fits to the NFW profile are rejected and not included in the catalogs. We believe that this is likely a major source of the incompleteness at $z > 2.5$. Note that the effect of this incompleteness is an underestimate of the number of low concentration halos.

5. RESULTS

5.1. Mass Functions

Several recent numerical studies have demonstrated that the J01 fitting formula for halo mass functions may, indeed, be considered "universal" as it accurately describes halo counts as a function of mass in N-body simulations of various cosmologies, including models containing dark energy with $w \neq -1$ and a time-varying w that is generically expected in the most common models of quintessence (Linder & Jenkins 2003; Klypin et al. 2003; Maccio et al. 2003; Lokas, Bode, & Hoffman 2003).

Here we confirm and further extend this conclusion by presenting halo mass functions from our simulations

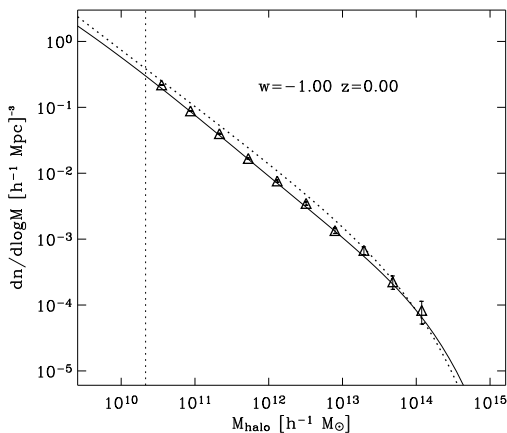


Fig. 6. The $z = 0$ CDM halo mass function of our simulation (triangles with error bars), compared to the PS (dotted) and J01 (solid) analytic formulae. The error bars on the simulated mass function correspond to the Poisson noise due to the finite number of halos per mass interval. The vertical dotted line at the left represents the low mass threshold for our FoF halos, equal to 20 particles. Only the $w = -1$ data are shown because the halo counts for $w \neq -1$ are nearly indistinguishable at $z = 0$.

at different redshifts. In Figure 6 we show the binned halo mass function for our CDM simulation. As Klypin et al. (2003) found, the mass functions for all values of w are nearly indistinguishable at $z = 0$, which is not surprising for very similar w , and the Jenkins formula provides an excellent approximation to the mass function in the simulation box. For reference, we also compare our simulation data to the Press & Schechter (1974, PS hereafter) mass function. Many previous studies (for a recent example, see Linder & Jenkins 2003 and references therein) have concluded that the PS mass function tends to overestimate the simulated halo mass function at the low mass ($M < M_c$) end and underestimate the number density of halos at the high mass ($M > M_c$) end. This trend is evident in Figure 6.

In Figure 7, we show the redshift evolution of the mass function for each w model separately. With the exception of the $w = -1.50$ case, all mass functions are described very well by the J01 formula out to $z = 3$. In the $w = -1.50$ case, the J01 mass function fits the data well out to $z < 1$, but over-predicts the number of halos at higher redshift. By $z = 1$, the difference between the simulated halo mass function and the J01 mass function is already a factor of 2 at the high mass end, and this discrepancy grows with increasing redshift.

5.2. Concentrations

In x3.2, we described the manner in which quintessence models test the predictions of the analytic B01 model for halo concentration as a function of mass. We have assembled catalogs consisting of more than 1600 halos for each of our quintessence N-body simulations. The density profiles of every halo have been fit to an NFW profile, and this profile has been used to calculate its virial mass and concentration. Some of these fits produced concentrations smaller than one, and we have excluded these halos from our subsequent analysis.

The resulting $c_{\text{vir}}(M_{\text{vir}})$ relations are plotted in Figure

8. We find that our simulations produce halos with slightly lower concentrations than expected from previous simulation results (e.g., B01, Colin et al. 2003) and from the original analytic model proposed by B01 with $F = 0.01$ and $K = 4.0$. However, we find that this difference can be described very well by a constant offset. For example, keeping $F = 0.01$ and lowering the proportionality constant K to $K = 3.5$ in the B01 model fits our data quite well for all of the w models we explore. We discuss this overall offset further in x5.3. The $c_{\text{vir}}(M_{\text{vir}})$ relation flattens out below $M_{\text{vir}} \approx 6 \times 10^{11} h^{-1} M_{\odot}$. We attribute this to the lower number of particles in these halos, making them more susceptible to relaxation effects, which tend to cause the central regions of halos to be more diffuse and lead to lower concentrations. It is thus unlikely that this flattening represents any physical effect (compare to the results of Colin et al. 2003), and we have neglected the lowest mass bin in determining the best-fit value of K .

As mentioned above (x3.2), considering several cosmological models with different virial overdensities δ_{vir} allows us to distinguish between analytic prescriptions based on definitions of halo concentration in terms of R_{200} , in which the proportionality constant K_{200} is independent of cosmology (Eq. 12), and those based on the virial radius R_{vir} , in which K_{vir} is cosmology-independent (Eq. 11). In order to test this we re-analyzed the five $z = 0$ N-body outputs using the BDM-like halofinder, but setting $\delta_{\text{vir}} = \delta_{\text{vir}} = b = \delta_{\text{vir}} = \delta_{\text{crit}} M^{-1} = 200 M^{-1} = 667$, effectively yielding a relation between c_{200} and M_{200} . Matching these relations to the model described by Eq. 12 we determined best-fit values of $K_{200} = (3.76; 3.44; 3.32; 3.16; 3.16)$ for $w = (-0.50; 0.75; 1.00; 1.25; 1.50)$. This range in K_{200} is not consistent with one cosmology-independent value of K_{200} , as predicted by the model based on a definition of concentration in terms of R_{200} . The results of this analysis seem to favor models similar to the B01 model, in which the halo concentration, defined in terms of R_{vir} as determined from a cosmology-dependent virial overdensity δ_{vir} , is related to $a = a_c$ via a cosmology-independent constant of proportionality K_{vir} . Put another way, defining the radius of a halo, and thus the concentration of a halo using a fixed overdensity criterion necessitates using a cosmology-dependent proportionality constant in Eq. (11) while the cosmology-dependent virial overdensity definition seems to account for these differences.

As in previous studies (B01; Jing 2000; Jing & Suto 2002) we also find that halos of a given mass have a distribution of concentrations. To determine the inherent scatter in the concentration-mass relation it is important to properly account for the artificial scatter introduced by uncertainties in the fit to an NFW profile and by Poisson noise in each bin. Following the B01 analysis, we have corrected for the former by determining 500 one-sided Gaussian deviates for each halo with a standard deviation equal to the error in the c_{vir} fit returned by the halofinder. The deviates are positive (negative) if c_{vir} is less (greater) than the median in that bin. We then determine the 16th and 84th percentiles in $\log(c_{\text{vir}})$ and subtract off the Poisson noise from each in quadrature. The resulting estimates of the intrinsic scatter are shown

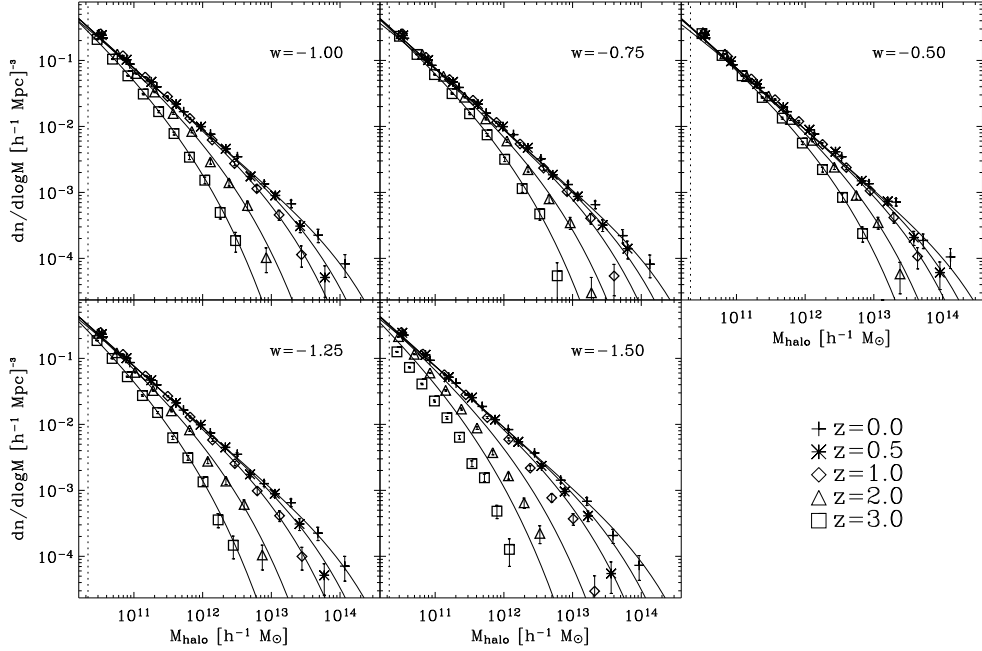


Fig. 7.1 A comparison between the J01 analytic mass function (solid lines) and the mass functions derived from our five N-body simulations (shapes with error bars, see the legend in the lower right portion of the Figure). The halos in our simulations were located using a FoF algorithm with a linking length equal to 0.2 times the mean particle separation as in J01. In each panel we plot mass functions at various redshifts, from top to bottom : $z = 0.0; 0.5; 1.0; 2.0$; and 3.0 . The error bars represent the Poisson noise due to the finite number of halos in each mass bin. Notice that the J01 mass function becomes an increasingly poor fit to the simulated mass functions for our $w = -1.5$ at high redshift.

as the dashed lines in Figure 8. The scatter is roughly independent of the value of w , and we find that taking the B01 proportionality constant to be $K_{\text{low}} = 2.28$ and $K_{\text{high}} = 4.52$ fits the lower and upper lines well. These values correspond to $\log c_{\text{low}} = 0.18$ dex and $\log c_{\text{high}} = 0.11$ dex. Although these are similar in magnitude to the scatter reported in previous studies, our distributions are skewed away from log-normal toward lower concentrations. We believe that this skewness is unphysical and may likely be caused by the lower resolution of our simulations, which tends to produce more low concentration halos.

For a fixed mass the B01 model predicts that concentration should decrease with redshift as $1/(1+z)$. The halos in our simulation also satisfy this relation, as shown by Figure 9, in which we plot the redshift dependence of concentration for halos of mass $M_{\text{vir}} = 7 \cdot 10^{11} h^{-1} M_{\odot}$. This figure shows that the concentrations follow the $c_{\text{vir}} / (1+z)^1$ relation that is embodied in the B01 analytic model. At redshifts greater than $z=2.5$ our catalogues of halos in this mass bin with fitted NFW profiles become incomplete. This incompleteness preferentially affects low concentration halos, causing the $c_{\text{vir}}(z)$ relation to attenuate at high redshift. We do not believe this to be a physical effect, and trust our data points only to $z=2.5$.

5.3. Exploring the Concentration Discrepancy

We have attempted to understand the origin of the discrepancy between $c_{\text{vir}}(M_{\text{vir}})$ derived from our simulations

and those found by B01 and given by the B01 analytic relation. We have reanalyzed the same $z=0$ simulation data that was analyzed previously by B01, and we were able to reproduce their $c_{\text{vir}}(M_{\text{vir}})$ relation and scatter. We conclude that the discrepancy that we observe is not due to any change in analysis procedures.

Of course, the main difference between the study of B01 and our work is the choice of simulation codes. Whereas we use the publicly-available, uniform-resolution code GADGET, B01 used the adaptive-refinement code ART. Undoubtedly the effective resolution at the centers of halos was higher in the B01 simulation than in ours.

In order to shed further light on this matter, we have run one additional GADGET simulation designed to provide a better match to the B01 ART simulation. Compared to the five simulations discussed previously, this new one has higher force resolution ($= 1.0 h^{-1} \text{kpc}$) and $\delta = 1.0$. The resulting $c_{\text{vir}}(M_{\text{vir}})$ relation is shown in Figure 10.

Here, too, we find that the GADGET concentrations are systematically lower than the ones found by B01 with ART by 14%. Instead of $K = 4.0$ we find $K = 3.44$ matches the GADGET halo concentrations. This is consistent with the value found for the five lower resolution quintessence simulations described above. It appears that the difference in K between our simulations and the B01 simulation may be due to an inherent difference between the GADGET and ART N-body codes. Whether this is due to the higher maximum force reso-

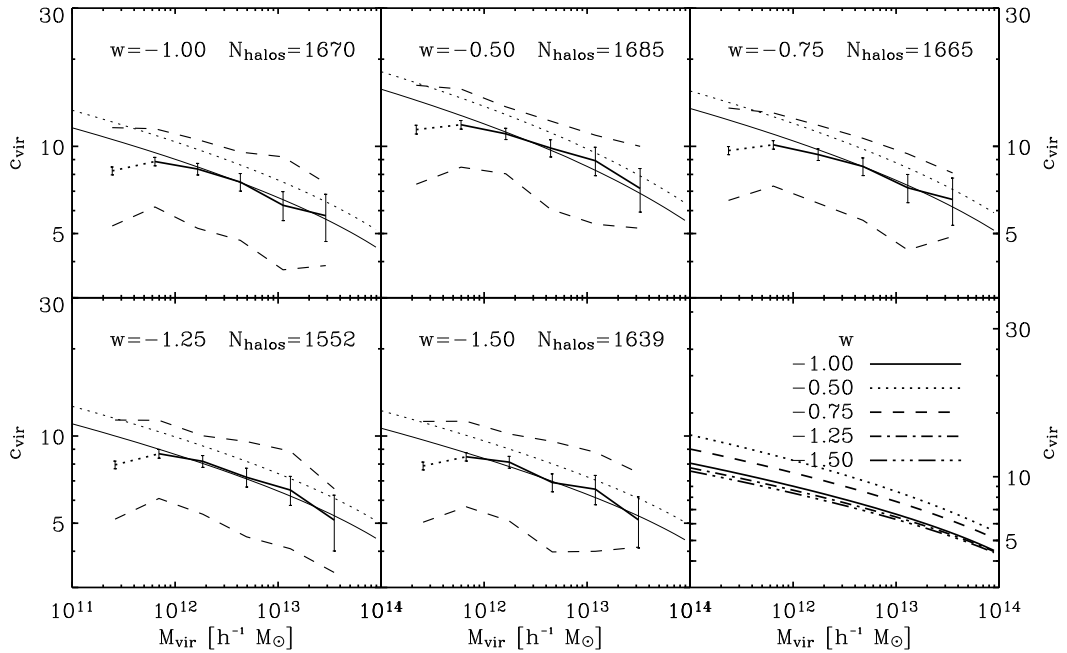


Fig. 8.1 The concentration parameter c_{vir} , as a function of mass M_{vir} , for the five quintessence N-body simulations. The original ($F = 0.01; K = 4.0$) and our best-fit ($F = 0.01; K = 3.5$) B01 models are over-plotted as thin dotted and solid lines, respectively. Error bars represent the Poisson noise due to the finite number of halos per bin. The dashed lines are our estimates of the intrinsic scatter in the relation, obtained by removing the scatter due to errors in the fits of the NFW profiles, as well as Poisson noise. The lowest mass bin was excluded in our analysis and is shown here for completeness only. The total number of halos in the remaining bins is shown in the upper right corner of each panel. The lower right panel shows the best-fit B01 model for all five values of w .

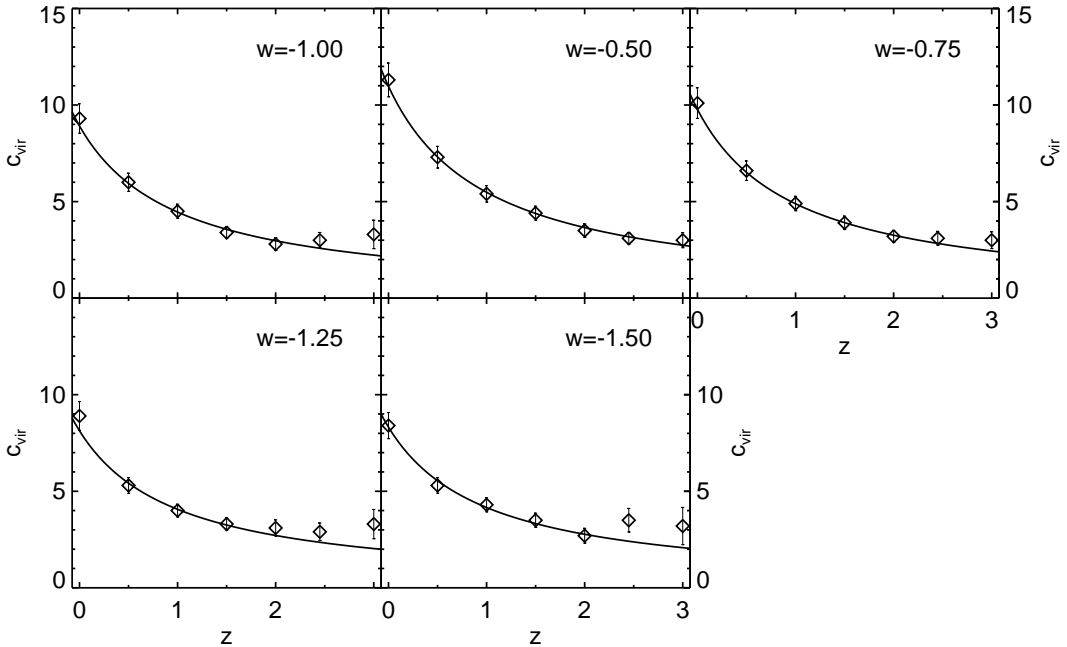


Fig. 9.1 The median concentrations of halos in bins of mass $M_{vir} = 7 \times 10^{11} h^{-1} M_\odot$ in 0.05 dex as a function of redshift. Error bars represent the Poisson noise due to the finite number of halos per bin. c_{vir} falls in proportion to $1/(1+z)$ (solid lines), in agreement with the B01 model. The flattening at $z > 2.5$ is probably not physical, and may be caused by incompleteness in the halo catalogs at high redshift which preferentially excludes low concentration halos.

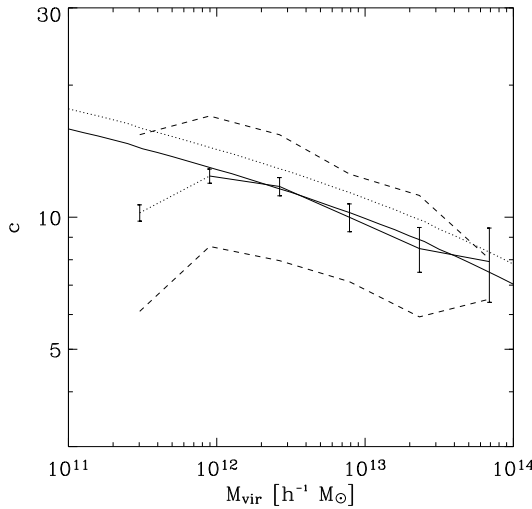


Fig. 10. | $c_{\text{vir}}(M_{\text{vir}})$ for our high resolution ($= 1.0 h^{-1} \text{kpc}$) $\sigma_8 = 1.0$ GADGET simulation designed to approximate the adaptive-re refinement ART simulation used in B01. The original B01 relation is overplotted as a dotted line. The dotted line segment and the dashed lines are as in Fig. 8.

lution a ordered by the adaptive refinement code ART or due to some other difference between the two codes is unclear.

Several recent analyses based on $w = 1$ simulations with higher resolution than our own (Hayashi et al. 2003, Colín et al. 2003, Tasitsiomi et al. 2003) also favor the B01 model with $K = 4.0$. In light of these results we conclude that the GADGET simulations systematically under-predict halo concentrations by 10–15%. However, when this offset is normalized out, the variation of $c_{\text{vir}}(M_{\text{vir}})$ with w scales as predicted, and we conclude that the B01 model is successful in this regard. Emboldened by this success, we use the model to explore the implications of various normalization choices and to compare expected halo densities with those inferred from galaxy rotation curves. In what follows, we assume $K = 4.0$ for the model normalization and we advocate this choice for the community for the reasons outlined above. (However, setting $K = 3.5$ would not change the conclusions that follow.)

6. HALO CONCENTRATIONS AND CENTRAL DENSITIES WITH $w \neq 1$

In Figure 11 we illustrate the degeneracy between w and σ_8 in setting halo concentrations. Shown are the predictions of the B01 model ($F = 0.01, K = 4.0$) for $c_{\text{vir}}(z = 0)$ with a fixed normalization $\sigma_8 = 0.74$ for several values of w . As discussed in x3.2, for a fixed normalization, concentrations increase as w increases because halos collapse earlier. The right panel of the figure shows the corresponding predictions for c_{vir} with σ_8 determined by normalizing to the CMB with $\sigma_8 = 1$ (see x2.3). Note that for the CMB normalization, the trend with w is in the opposite direction, with increasing w implying lower concentrations. As illustrated in Figure 2, higher w requires a lower normalization: $\sigma_8' = 0.6, 0.9$, and 1.0 for $w = 0.5, 1$, and 1.5 , respectively. The change in normalization based on the CMB is more important

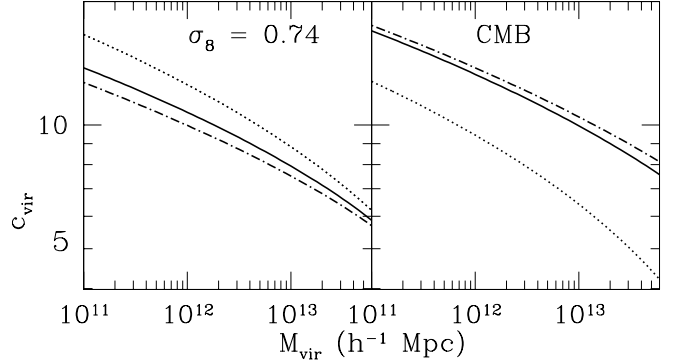


Fig. 11. | Predictions for halo concentration as a function of M_{vir} . Dotted, solid, and dash-dot lines in each panel refer to $w = 0.5, 1$, and 1.5 , respectively. The left panel is for the fixed σ_8 used in the simulations presented in this paper. The right panel shows the halo concentration changes when we normalize based on the CMB: $\sigma_8' = 0.6, 0.9$, and 1.0 for $w = 0.5, 1$, and 1.5 , respectively.

than the changes in the growth function that give rise to the behavior of $c_{\text{vir}}(w)$ at fixed normalization.

As discussed previously, the c_{vir} parameter is useful for theoretical reasons, but it is not a direct indicator of physical density. We would like, therefore to convert our predicted c_{vir} relations into quantities that have a more direct physical meaning, and that are also more amenable to comparison with observations. Abram, Bullock, & Weinberg (2002) proposed the so-called central density parameter as a means to quantify the physical density in the central regions of a galaxy:

$$v_{=2} = \frac{1}{2} \frac{V_{\text{max}}}{H_0 r_{v=2}}^2 : \quad (14)$$

$v_{=2}$ is defined as the mean overdensity within $r_{v=2}$, the radius at which the galaxy rotation curve reaches one-half its maximum observed velocity V_{max} .

The $v_{=2}$ parameter is advantageous for several reasons. First, it facilitates comparisons between theory and observation. Any predicted c_{vir} vs. M_{vir} relation can be easily converted into a $v_{=2}$ vs. V_{max} relation. Similarly, given an observed galaxy rotation curve, $v_{=2}$ can be determined without reference to any particular analytic density profile. It also has the useful characteristic that even if an observed rotation curve is rising at the last measured point, substituting the highest (outer) measured point on the rotation curve for V_{max} in the formula above results in an upper limit on the true value of $v_{=2}$. Specifically, if V_{max} is underestimated by a factor f_v , and the density profile varies with radius as $(r)/r^2$, this leads to an overestimate of $v_{=2}$ by a factor of $f_v^{-2} = (2)^2$. Thus this is an overestimate so long as the density profile falls off with radius or is constant. Furthermore, if $f_v > 2=3$, the fractional overestimate of $v_{=2}$ is larger than the fractional underestimate of V_{max} .

We compare the B01 model predictions in terms of these quantities in Figure 12 for three representative quintessence cosmologies to the observational data of low-surface brightness and dwarf galaxies compiled in Zentner & Bullock (2002), the same set of observed galaxies are discussed in Hayashi et al. 2003, who reach sim-

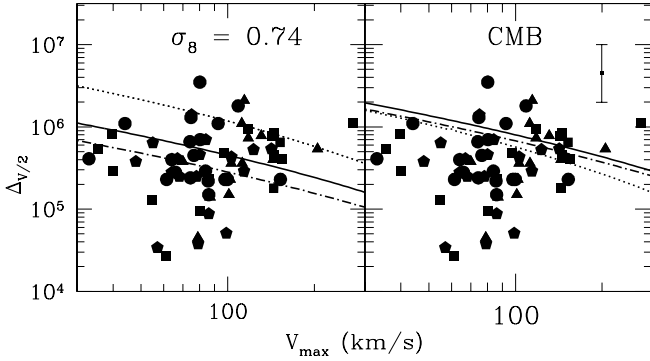


Fig. 12.] The central density parameter as a function of the maximum halo circular velocity. Dotted, solid, and dash-dot lines in each panel refer to $w = 0.5$, 1 , and 1.5 , respectively. The left panel is for a fixed $\sigma_8 = 0.74$ and the right panel is normalized to match the CMB: $\sigma_8 = 0.6$, 0.9 , and 1.0 for $w = 0.5$, 1 , and 1.5 , respectively. The error bar in the right panel shows the expected theoretical 1-sigma scatter in $v_{=2}$ due to the scatter in c_{vir} . The points are for observed LSB and dwarf galaxies (see text for references).

ilar conclusions) from the observational work of Swaters (1999), de Blok, McGaugh, & Rubin (2001), and de Blok and Bosma (2002). The error bar in the right panel shows the theoretical 1-sigma scatter in $v_{=2}$ expected at fixed velocity due to the scatter in c_{vir} .

While it is difficult to quantify the agreement of each quintessence cosmology with observational data, the cosmological model that is most commonly referred to as the standard, concordance cosmological model with $w = 1$ ($\sigma_8 = 0.9$ (solid line, right panel) seems to be in conflict with the extant observational data. For $w = 1$, lowering the normalization of the power spectrum to the value $\sigma_8 = 0.74$ (solid line, left panel) can greatly alleviate this discrepancy (Aram, Bullock, & Weinberg 2002; Zentner & Bullock 2002; McGaugh et al. 2003). However, a $w = 0.5$ model with the same $\sigma_8 = 0.74$ normalization (dotted line, left panel) does not do as well because earlier structure formation produces higher galactic central densities.

Notice that the trends with $v_{=2}$ for fixed V_{max} do not scale as might be expected from the c_{vir} trends at fixed mass shown in Figure 11. This is because $v_{=2}$ is a physical measure of density and it increases not only with c_{vir} but also with V_{vir} . This effect is most apparent when comparing the right-hand panels of Figures 11 and 12. Specifically, even though the concentrations of halos with $w = 0.5$ and $\sigma_8 = 0.6$ (dotted-line, right panel, Figure 11) are much lower than those in the standard $w = 1.0$, $\sigma_8 = 0.9$ case (solid line, right panel), the actual densities of those halos are roughly the same in the right panel of Figure 12. This is because $w = 0.5$ models have higher virial densities (see Figure 4). Even though halos in the low-normalization $w = 0.5$ model tend to have the same (rapid-collapse) formation epoch as those in the higher-normalization $w = 1$ model, the higher virial densities in the former model make the halos denser overall.

By inspecting Figure 12 we can immediately determine that models with $w < 1$ and moderately low σ_8 ($\sigma_8 = 0.7$ – 0.8) can bring theoretical predictions to

rough agreement with rotation curve data from low surface brightness and dwarf galaxies. Though it is clear that sufficiently decreasing σ_8 can bring any model in accord with the median of the data, a $w = 0.5$ model would require $\sigma_8 < 0.6$. Such a low normalization would be nearly impossible to reconcile with $z = 0$ cluster abundance data. Thus from the standpoint of quintessence, models with $w < 1$ seem favored by galaxy density data. Conversely, models with w as low as 0.5 are disfavored by galactic rotation curves coupled with only a very weak prior on the normalization of the power spectrum.

Note that none of the models can easily account for the some of the very low data points. Nevertheless, the scatter in the data is not extremely large compared to the scatter expected from the halo-to-halo variations observed in N-body simulations. For example, at $V_{\text{max}} = 80$ km/s, the 1-sigma scatter in N-body simulations is $(\log(v_{=2}))' = 0.37$ while the 1-sigma scatter in all 67 data points is $(\log(v_{=2}))' = 0.41$. This suggests that lowering the median of the theoretically predicted central densities, perhaps by a reduction in σ_8 or invoking a tilted or running power spectrum that reduces power on galaxy scales, or as we discuss here, even by invoking $w < 1$ quintessence, may be sufficient to bring the predictions into good agreement with the data. However, we must bear in mind that our calculations are approximate. The most obvious omission is that all of our calculations are based on N-body simulations that contain no baryons. Note that the effects of baryonic contraction are likely to be small in LSB galaxies (e.g., de Blok & McGaugh 1997) and would tend to drive rotation curves to higher values of $v_{=2}$ and V_{max} in the simplest models (Bullock et al. 1986). This serves only to increase the apparent discrepancy. Additionally, rotation curve measurements may yet be subject to poorly-understood systematic effects in the reduction of the observational data (Swaters et al. 2003). At this point it is difficult to draw a firm conclusion.

7. SUMMARY AND CONCLUSIONS

Although the nature of dark energy is unknown, its effects on structure formation can be studied using numerical N-body simulations. We have performed a series of these simulations for a range of dark energy equation of state parameters. Continuing previous findings by Linder & Jenkins (2003), Klypin et al. (2003), Maccio et al. (2003), and Lokas et al. (2003) we show that the J01 formula provides a good fit to halo mass functions even in the presence of non-CDM dark energy. We show that, at least at low redshift ($z < 0.5$) this is true for models with $w < 1$ as well. At higher redshifts ($z > 1$) we find a potential conflict between our simulation results and the J01 mass function for our $w = 1.5$ model. Further study is needed in order to confirm this preliminary conclusion.

The density structure of dark matter halos is also affected by dark energy. We have shown how the predictions of the J01 model are modified when dark energy with constant w is accounted for. As structure tends to form earlier in models with less negative w , halo concentrations tend to be somewhat higher in these models. These findings are in agreement with the results of

Klypin et al. (2003) and qualitatively agree with Dolag et al. (2003), although we probe a different range of masses than the latter. The larger number of halos with NFW profiles and concentrations in our study allows us to quantitatively test the B01 model. We find that the original ($F = 0.01; K = 4.0$) over-predicts the concentrations of halos in our simulations by about 12–15%. However, the shape of the mass-concentration relation that we find is the same as in B01, and we find that a slightly modified set of the B01 parameters ($F = 0.01; K = 3.5$) matches our halos well. This offset may likely be caused by the lower force resolution of our GADGET simulations compared to the adaptive refinement code ART used in B01. For the halos in our simulations the adopted B01 model accurately reproduces the median concentration-mass relation over a range of masses from $M_{\text{vir}} = 6 \cdot 10^{11}$ to $M_{\text{vir}} = 4 \cdot 10^{13} h^{-1} M_{\odot}$. We confirm that for a fixed mass halo concentration decrease with redshift as $1 = (1 + z)$, at least out to $z = 2.5$.

Interestingly, we find that halo concentrations are more easily understood when the halo virial radius is defined in terms of a cosmology-dependent virial overdensity rather than by one that uses a fixed overdensity of $\delta = \delta_{\text{crit}} = 200$. The result supports one of the (previously-untested) assumptions of the original B01 model. Specifically, we argue that halo densities in different cosmological models are influenced both by changes in the overall virialization process of halos as well as by changes in epoch when the halo cores collapse. As noted in x6, it is important to include both of these physical processes when comparing predictions for galaxy densities to real data, as in Figure 12.

Having confirmed that the B01 model correctly describes the scaling of halo concentrations as a function of mass and redshift even in cosmologies with $w \neq -1$, we have investigated the effects of dark energy on a comparison between model predictions and observations of central halo densities. Zentner and Bullock (2002) found that the observed distribution of $v_{\text{max}} = 2$ as a function of V_{max} is inconsistent with the predictions of the B01 model for CDM and $w = 0.9$. The model predicts halos that are simply too concentrated (see also Primack 2003). A lower value of $w = 0.75$, as used in our simulations, can alleviate this discrepancy, but such models may face other difficulties regarding early reionization (Somerville, Bullock, & Livio 2003) and possibly with reproducing the properties of halo substructure (Zentner & Bullock 2003). Including the effects of dark energy, we find that for models with $w > -1$ the problem is exacerbated because halos collapse earlier and because they

have higher virial overdensities. Note that for the extreme case of $w = -0.5$, even a normalization as low as $\delta = 0.6$ seems disfavored by the data. Thus one interesting conclusion is that the rotation curves of galaxies coupled only with a weak prior on the normalization of the power spectrum of density fluctuations seem to disfavor quintessence models with w significantly larger than

1 without measuring the expansion history of the Universe, as is done in SN Ia analyses. Models with $w < -1$ do better, and can tolerate higher values of $\delta = 0.8$, but not high as high as $\delta = 1$, as is suggested the CMB normalization.²

In this paper we have shown how simple models of dark energy affect the abundance and concentration of dark matter halos. We have shown that our current understanding of halo mass functions and concentrations, derived from CDM simulations, can be extended to describe halos in universes with constant $w \neq -1$ with perhaps one exception for very low w . Our results only pertain to halos with masses between $7 \cdot 10^{11}$ to $4 \cdot 10^{13} h^{-1} M_{\odot}$, only at redshifts < 2.5 , and neglect the effect of cooling baryons on dark matter profiles. As future observations further constrain the nature of dark energy, it will become necessary to extend these tests to more realistic models of dark energy. Future simulations with higher mass and force resolution, including the effects of baryons, and incorporating more realistic dark energy models will further advance our understanding of the interplay between cosmology and dark matter halo structure.

We thank P. Madau for interesting and helpful discussions. M.K. is supported by NSF grant AST-0205738. L.E.S. is supported by the Department of Energy grant DE-FG 02-91ER40690. A.R.Z. is supported by The Center for Cosmological Physics at The University of Chicago under NSF PHY 0114422. J.S.B. is supported by NASA through Hubble Fellowship grant HF-01146.01-A from the Space Telescope Science Institute, which is operated by the Association of Universities for Research in Astronomy, Incorporated, under NASA contract NAS5-26555. J.R.P. is supported by NSF grant AST-0205944. A.R.Z. thanks The Center for Cosmology and Particle Physics at New York University for their hospitality during several visits while this work was in progress. We thank V. Springel for use of the publicly-available code GADGET and we thank U. Seljak and M. Zaldarriaga for use of the publicly-available code CMBFAST.

REFERENCES

Alam, S.M., Bullock, J.S., & Weinberg, D.H. 2002, ApJ, 572, 34
 Allen, P.R., Trilling, D.E., Koemer, D.W., & Reid, I.N. 2003, ApJ, 595, 1206
 Barris, J.B., et al. 2003, ApJ, accepted (preprint: astro-ph/0310843)
 Bartelmann, M., Perrotta, F., & Baccigalupi, C. 2002, A & A, 396, 21
 Bum enthall, G.R., Faber, S.M., Flores, R., & Primack, J.R. 1986, ApJ, 301, 27
 Bucher, M., & Spergel, D. 1999, Phys. Rev. D, 60, 043505
 Bullock, J.S., et al. 2001, MNRAS, 321, 559 (B01)
 Bullock, J.S. 2002, The shapes of galaxies and their dark halos, Proceedings of the Yale Cosmology Workshop "The Shapes of Galaxies and Their Dark Matter Halos", New Haven, Connecticut, USA, 28–30 May 2001. Edited by Priyamvada Natarajan. Singapore: World Scientific, 2002, ISBN 9810248482, p.109, 109
 Caldwell, R.R. 2002, Phys. Lett. B, 545, 23
 Caldwell, R.R., Dave, R., & Steinhardt, P.J. 1998, Phys. Rev. Lett., 80, 1582
 Carlstrom, J.E., Holder, G., and Reese, E.D. 2001, ARAA, 40, 643
 Carroll, S.M., Homan, M., & Trodden, M. 2003, Phys. Rev. D, 68, 023509

Colin, P., Klypin, A. A., Valenzuela, O., & Gottlöber, S. 2003, *ApJ*, submitted, (preprint: astro-ph/0308348)

Dave, R., Caldwell, R. R., & Steinhardt, P. J. 2002, *Phys. Rev. D*, 66, 023516

Davis, M., Efstathiou, G., Frenk, C. S., White, S. D. M. 1985, *ApJ*, 292, 371

de Blok, W. J. G. & McGaugh, S. S. 1997, *MNRAS*, 290, 533

de Blok, W. J. G., McGaugh, S. S., & Rubin, V. C. 2001, *AJ*, 122, 2396

de Blok, W. J. G., Bosma, A. A., & McGaugh, S. S. 2003, *MNRAS* 340, 657

Dodelson, S., et al. 2002, *ApJ*, 572, 140

Dolag, K., et al. 2003, *A&A*, submitted (preprint: astro-ph/0309771)

Eke, V. R., Navarro, J. F., Steinmetz, M. 2001, *ApJ*, 554, 114

Flores, R., Bullock, J. S., Kravtsov, A. V., & Primack, J. R. 2004, in preparation

Ghigna, S., Moore, B., Governato, F., Lake, G., Quinn, T., Stadel, J. 1998, *MNRAS*, 300, 146

Hayashi, E., et al. 2003, *MNRAS*, submitted (preprint: astro-ph/0310576)

Hoekstra, H., Yee, H. K. C., & Gladders, M. D. 2003, *ApJ* submitted (preprint: astro-ph/0306515)

Hu, W., & Sugiyama, N. 1995, *ApJ*, 444, 489

Hu, W., & Jain, B. 2003, *Phys. Rev. D*, submitted (preprint: astro-ph/0312395)

Huterer, D., & Ma, C.-P. 2004, *ApJ*, 600, L7

Jenkins, A., et al. 2001, *MNRAS*, 321, 372 (J01)

Jing, Y. P. 2000, *ApJ*, 535, 30

Jing, Y. P., & Suto, S. 2002, *ApJ*, 574, 538

Klypin, A. A., & Holtzman, J. 1997, astro-ph/9712217

Klypin, A. A., Kravtsov, A. V., Bullock, J. S., & Primack, J. R. 2001, *ApJ*, 554, 903

Klypin, A. A., Maccio, A. V., Mainini, R., Bonometto, S. A. 2003, *ApJ*, 599, 31

Knop, R. A. et al. 2003, *ApJ*, 598, 102

Kravtsov, A. V., Klypin, A. A., Kholhlov, A. M. 1997, *ApJS*, 111, 73

Kuhlen, M., Keeton, C. R., & Madau, P. 2004, *ApJ*, 601, 104

Kujat, J., Linn, A. M., Scherrer, R. J., & Weinberg, D. H. 2002, *ApJ*, 572, 1

Lacey, C. & Cole, S. 1993, *MNRAS*, 262, 627

Lee, J., & Shandarin, S. F. 1999, *ApJ*, 517, L5

Linder, E. V., & Jenkins, A. 2003, *MNRAS*, 346, 573

Lokas, E. L., Bode, P., & Homan, Y. 2003, *MNRAS*, submitted (preprint: astro-ph/0309485)

Ma, C.-P. & Bertschinger, E. 1995 *ApJ*, 455, 7

Ma, C.-P., Caldwell, R. R., Bode, P., & Wang, L. 1999 *ApJ*, 521, L1

Maccio, A. V., Quercellini, C., Mainini, R., Amendola, L., & Bonometto, S. A. 2003, *Phys. Rev. D*, submitted (preprint: astro-ph/0309671)

Molinari, E., & Zacchei, A. 2002, *ApJ*, 575, 801

McGaugh, S. S., Barker, M., & de Blok, W. J. G. 2003, *ApJ*, 584, 566

Monaco, P. 1995, *ApJ*, 447, 23

Navarro, J. F., Frenk, C. S., & White, S. D. M. 1995, *MNRAS*, 275, 56

Navarro, J. F., Frenk, C. S., & White, S. D. M. 1996, *ApJ*, 462, 563

Navarro, J. F., Frenk, C. S., & White, S. D. M. 1997, *ApJ*, 490, 493

Navarro, J. F., et al. 2003, *MNRAS*, submitted (preprint: astro-ph/0311231)

Perlmutter, S., et al. 1999, *ApJ*, 517, 565

Pierpaoli, E., Scott, D., & White, M. 2001, *MNRAS*, 325, 77

Pierpaoli, E., Borgani, S., Scott, D., & White, M. 2003, *MNRAS*, 342, 163

Power, C., Navarro, J. F., Jenkins, A., Frenk, C. S., White, S. D. M., Springel, V., Stadel, J., & Quinn, T. 2003, *MNRAS*, 338, 14

Press, W. H., & Schechter, P. 1974, *ApJ*, 187, 425

Primack, J. R. 2003, *IAU 220 Proceedings* (preprint: astro-ph/0312459)

Ratra, B. & Peebles, P. J. E. 1988, *Phys. Rev. D*, 37, 3406

Reiprich, T. H., & Böhringer, H. 2002, *ApJ*, 567, 716

Riess, A. G., et al. 2001, *ApJ*, 560, 49

Sarbu, N., Rusin, D., & Ma, C.-P. 2001, *ApJ*, 561, L147

Schuecker, P., Caldwell, R. R., Böhringer, H., Collins, C. A., Guzzo, L., Weinberg, N. N. 2003, *A&A*, 402, 53

Seljak, U. 2002, *MNRAS*, 337, 769

Seljak, U., & Zaldarriaga, M. 1999, *ApJ*, 469, 437

Sheth, R. K., & Tormen, G. 1999, *MNRAS*, 308, 119

Silveira, V., & Waga, I. 1994, *Phys. Rev. D*, 50, 4890

Somerville, R. S., Bullock, J. S., & Livio, M. 2003, *ApJ*, 593, 616

Spergel, D. N., et al. 2003, *ApJS*, 148, 175

Springel, V., Yoshida, N., White, S. D. M. 2001, *New Astronomy*, 6, 51

Swaters, R. A. 1999, PhD Thesis, University of Groningen

Swaters, R. A., M. Adore, B. F., van den Bosch, F. C., & Baloëlls, M. 2003, *ApJ*, 583, 732

Tegmark, M. et al. 2003a, (preprint: astro-ph/0310723)

Tegmark, M. et al. 2003b, (preprint: astro-ph/0310725)

Tassis, I. A., Kravtsov, A. V., Gottlöber, S., & Klypin, A. A., 2003 (preprint: astro-ph/0311062)

Wang, L., & Steinhardt, P. J. 1998, *ApJ*, 508, 483

Weldner, R. H., Bullock, J. S., Primack, J. R., Kravtsov, A. V., & Dekel, A. 2002, *ApJ*, 568, 52 (W02)

Weinberg, N. N., & Kamionkowski, M. 2003, *MNRAS*, 341, 251

Zentner, A. R., & Bullock, J. S. 2002, *Phys. Rev. D*, 66, 043003

Zentner, A. R., & Bullock, J. S. 2003, *ApJ*, 598, 49

Zhao, D. H., Jing, Y. P., Mo, H. J., & Bomer, G. 2003, *ApJ*, 597, L9